

Change in atomic coordination in a heavily deformed metallic glass

Y. Liu,^{1,2} G. Schumacher,² H. Riesemeier,³ and J. Banhart^{2,4}

¹Key Laboratory for Liquid-Solid Structural Evolution and Processing of Materials, Ministry of Education, Shandong University, Jinan 250061, People's Republic of China

²Helmholtz-Zentrum Berlin für Materialien und Energie GmbH, Hahn-Meitner Platz 1, D-14109 Berlin, Germany

³Bundesanstalt für Materialforschung und -prüfung, Unter den Eichen 87, D-12205 Berlin, Germany

⁴Technische Universität Berlin, Materials Science and Technology, Hardenbergstr. 36, 10623 Berlin, Germany

(Received 23 April 2014; accepted 13 May 2014; published online 28 May 2014)

The local structure around Ni and La atoms in Al₈₅Ni₁₀La₅ amorphous powder after ball milling was investigated by X-ray absorption spectroscopy. A continuous decrease in coordination number of Ni and La as a function of milling time was observed, while the nearest neighbour distance and the mean square atomic displacement did not change, pointing at the creation of free volume around the Ni and La atoms. These structural changes resemble those of a liquid upon temperature increase. The results are described by a shear band model in which the coordination numbers of Ni and La are different within and outside a shear band. © 2014 AIP Publishing LLC. [<http://dx.doi.org/10.1063/1.4879682>]

I. INTRODUCTION

The combination of high strength and extended elastic range makes metallic glasses potential structural materials. Unfortunately, the correlation between mechanical properties and atomic structure in metallic glasses is still poorly understood, which hinders systematic development.¹ Recently, progress has been made in the understanding of the elastic properties of metallic glasses. Based on comparisons of both Young's and shear moduli of a series of metallic glasses with those of the alloy components, it was found that the elastic moduli of these glasses are primarily determined by their solvent elements.² Solute-centred clusters hardly influence elasticity while solvent-rich configurations in between the solute-centred clusters preferentially accommodate elastic strain. This preferential straining of solvent-rich areas is ascribed to a hierarchy of bonding forces: the strong interaction between solute and solvent atoms that give rise to solute-centred clusters and the weaker solvent-solvent bonds linking such clusters.² *In-situ* neutron diffraction experiments on elastically strained amorphous alloys revealed a shift of the first sharp diffraction peak in the structure factor. This shift was assigned to changes at the medium-range scale (0.4 nm to 2 nm), pointing at heterogeneous elastic straining² on the MRO scale in between the solute-centred clusters. A heterogeneous structure was also employed to explain the elastic behaviour of a Zr-based bulk metallic glass.³ It was shown by diffraction of high energy synchrotron radiation (120 keV) that the response of the alloy to external load is elastic by about 75% and anelastic by about 25%. The anelastic regions bear no static shear load.³

Based on results obtained from dynamic micropillar tests on a Zr-based bulk metallic glass, a viscoelastic core-shell model was suggested consisting of a soft free-volume rich zone in the core and surrounding tightly bound atomic clusters.¹ While the free-volume zones of the core show Newtonian flow, the elastic atomic clusters of the shell

exert back-stresses on the free-volume rich zones such that the original configuration can be restored by Newtonian flow.

The progress in describing elastic and viscoelastic properties in terms of heterogeneous structures consisting of hard clusters and soft free-volume zones suggests that other mechanical properties, such as yield strength and plasticity, are also related to structural heterogeneities.⁴ Furthermore, such heterogeneity of structure raises questions concerning the localization of damage after plastic deformation.

Unlike crystalline materials where plastic deformation proceeds via creation and slip of dislocations, plastic deformation in metallic glasses at temperatures below about $T = 0.9T_g$ (T_g : glass transition temperature) proceeds via formation of shear bands⁵ with typical shear band thicknesses between 10 nm and 20 nm.⁶⁻⁹ In the past years, the structure of shear bands has been the subject of intensive investigations. Cahn *et al.* pointed out that dilatation inside a shear band must be some percent.¹⁰ This is supported by a strongly enhanced diffusivity in plastically deformed Al₈₈Y₇Fe₅ glasses, which was ascribed to the excess free volume induced in shear bands by plastic deformation.¹¹ The local increase in free volume within shear bands due to plastic strain is in agreement with the free-volume model of Spaepen for anelastic flow¹² and with the model of argon for plastic deformation.¹³

In some Al-based alloys, the large atomic mobility inside the shear bands during deformation leads to the formation of fcc Al nanocrystals.^{11,14,15} The mechanism by which crystallization in shear bands occurs is still under discussion.⁵ Athermal,^{11,16} thermal,¹⁷ or combined athermal and thermal mechanisms¹⁸ have been suggested to explain the formation of nanocrystals in shear bands during plastic deformation. Despite an appreciable amount of work on the structure of shear bands has been done, the mechanisms of plastic deformation are still not understood in detail.

Metallic glasses do not exhibit long-range order (LRO). Their structure is described by short-range order (SRO) and

medium-range order (MRO). X-ray absorption spectroscopy (XAS) provides information about the number of nearest neighbours Z , the interatomic distance D , and the mean squared relative displacement of the effective interatomic distance σ^2 . The latter parameter is often denoted as “disorder parameter.” XAS is therefore an established method to describe SRO in metallic glasses, while MRO (about 0.4 nm–2 nm) is described by pair distribution functions measured by diffraction of X-rays or neutrons over a large range in reciprocal space.

Here, we present a systematic investigation of SRO of amorphous He-atomized $\text{Al}_{85}\text{Ni}_{10}\text{La}_5$ powder after different levels of plastic deformation. XAS is employed to follow the changes in SRO. Our results give evidence for the change in coordination numbers around Ni and La atoms. This points at the creation of free volume in Ni and La-centred clusters which approach a saturation concentration at large ball milling times. The results will be discussed applying a shear band model, which assumes maximum damage within each shear band.

II. EXPERIMENTAL

An alloy with the nominal composition $\text{Al}_{85}\text{Ni}_{10}\text{La}_5$ (at. %) was synthesized in an alumina crucible by induction melting pure elements of Al (99.98%), Ni (99.7%), and La (99.7%) under argon atmosphere. The melt was heated up to approximately 1200 °C and was subsequently atomized with helium gas at Nanoval GmbH applying their “Nanoval” process.¹⁹ As-atomized powder was plastically deformed by ball milling at room temperature in argon atmosphere for different ball milling times t using a Spex Mixer Mill 8000. The powder mass for each milling run was 6.2 g (corresponding to 1.77 cm³) resulting in a mass ratio between the ZrO_2 balls and the powder charge of 2:1. The milling process was terminated after different times (60 min, 120 min, 240 min, 600 min, and 6000 min) after which small amounts of the powder were used for X-ray diffractometry (XRD), differential scanning calorimetry (DSC) analysis, and XAS.

The local atomic structure around Ni and La atoms was investigated by XAS at the BAMline, BESSY II, Berlin, Germany. Extended X-ray Absorption Fine Structure (EXAFS) data were collected around Ni and La K-edges in the transmission mode using double multilayer monochromator which can provide an energy bandwidth of 1.7% in the range between 5 keV and 50 keV. Reference samples of bulk Ni (5- μm -thick foil), La_2O_3 (powder size less than 20 μm , deposited on 4 layers of Kapton tape) served as standards for comparison purposes and subsequent data analysis. The measured EXAFS spectra were transformed into k -space using the combined programs *ATHENA* and *ARTEMIS*.²⁰ The structural data needed for calculating the fitting standards were prepared using the program *ATOMS*,²¹ while theoretical scattering paths were calculated with the *ab-initio* program *FEFF*.²² Structural data for generating theoretical standards were selected on the basis of inspection of atomic positions in the binary crystalline phases NiAl_3 and LaAl_3 , respectively. The Fourier transformed (FT) EXAFS data were fitted

with a single shell model from 1.2 Å to 2.8 Å on Ni edge and from 1.7 Å to 3.5 Å on La edge, respectively.

DSC experiments were carried out in a Perkin-Elmer Pyris-1 under a stream of argon gas during continuous heating at 20 K/min. Second-run data in which the samples had already fully crystallized provided the baselines. The amorphous nature in the as-atomized state was confirmed by X-ray diffraction²³ and transmission electron microscopy.

III. RESULTS

Fig. 1 displays the magnitude of the Fourier transformed EXAFS signals $FT(k^2 \cdot \chi(k))$ for the as-atomized and ball-milled powders. All the spectra have a similar appearance, featuring a maximum near $R = 2$ Å. Above $R \approx 2.5$ Å, $FT(k^2 \cdot \chi(k))$ exhibits only small undulations, indicating the lack of strong structural correlations beyond the first shell. The peak value of $FT(k^2 \cdot \chi(k))$ decreases monotonically with ball milling time, see inset of Fig. 1, while thermal treatment of powder ball-milled for 120 min and subsequently annealed for 10 min at 150 °C restores the amplitude back to the value corresponding to 60 min of ball-milling. The area under the peak at $R \approx 2$ Å in $FT(k^2 \cdot \chi(k))$ reflects the number of nearest neighbours and their disorder around Ni. The decreasing maximum value of $FT(k^2 \cdot \chi(k))$ with longer ball-milling time thus indicates a decrease of the coordination number Z , whereas thermal treatment of ball-milled material causes an increase in Z .

The EXAFS spectra of the as-atomized powder along with the single-shell fit to the data are shown in Fig. 2(a), the magnitude and imaginary part of its Fourier transform in Fig. 2(b). The fits to the data of all the other specimens are of similar quality and are not shown here. The coordination number Z around Ni atoms as obtained by data fitting is about 6 in the as-atomized condition and decreases continuously with increasing ball milling time, see Fig. 3(a), while D and σ^2 remain unchanged within the experimental accuracy, see Table I. A decrease in Z at constant D and σ^2 was also observed for the coordination around La atoms, see Fig. 3(b) and Table I.

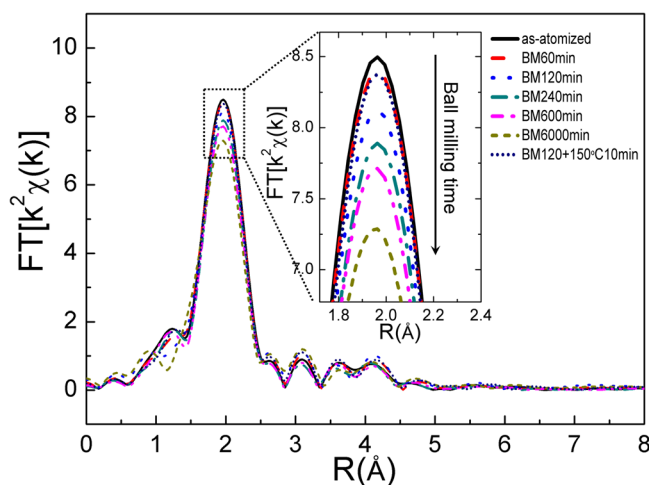


FIG. 1. FT of the k^2 -weighted EXAFS signals $\chi^2(k)$ of He-atomized $\text{Al}_{85}\text{Ni}_{10}\text{La}_5$ powder in the as-atomized condition and after ball milling for different times. The inset is a magnification of the first maximum in the FT.

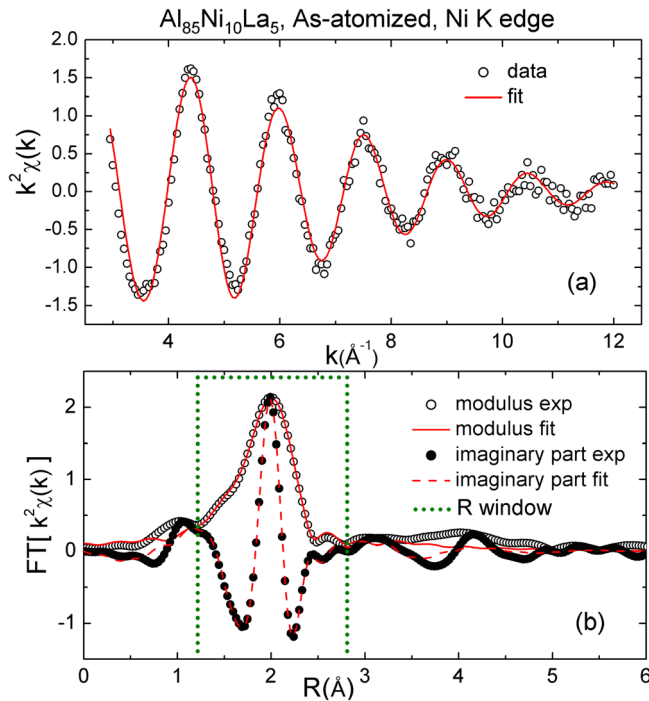


FIG. 2. k^2 -weighted EXAFS spectrum of the as-atomized powder (a) and corresponding FT (b), the latter being represented by the magnitude and imaginary part of the FT. Various lines represent fitted curves based on a single-shell model.

The heat flow during continuous heating as a function of temperature for different ball milling times is shown in Fig. 4(a). The DSC trace of the as-atomized powder reveals an exothermic reaction between about 100°C and the onset of glass transition $T_{g,o}$ ($T_{g,o} = 253.5^\circ\text{C}$, see Ref. 23), which reflects the annihilation of free volume in the as-atomized state. The amount of heat released below $T_{g,o}$ increases continuously during ball milling, while the endothermic reaction reflecting the glass transition gradually vanishes.

Fig. 4(b) shows the released heat integrated from 100°C to $T_{g,o}$ as a function of the number of impacts of a ball with the container wall n . The dashed line in Fig. 4(b) represents an exponential fit to the data according to

$$\Delta H = \Delta H_{BM}^{max} - \Delta H_{BM}^{max} \cdot \exp(-\beta_{\Delta H} \cdot n), \quad (1)$$

where $\Delta H_{BM}^{max} = \Delta H_{aa} + \Delta H_{BM}^{max}$ denotes the maximum heat release, ΔH_{BM}^{max} is the maximum heat release caused by deformation, and ΔH_{aa} is the heat release of the as-atomized powder. $\beta_{\Delta H}$ is a parameter that describes the relative heat release induced by the first impact through plastic deformation. The number of impacts of a ball with the container wall, n , is given by

$$n = 2 \cdot t \cdot m_B \cdot f, \quad (2)$$

where m_B is the number of balls in the mill and f is the rotational frequency of the SPEX mill. In our experiment, $m_B = 2$ and $f = 17 \text{ s}^{-1}$. The factor of 2 in Eq. (2) takes into account that with each back-and-forth swing of the vial the balls collide twice with opposite ends of the vial. The fit to

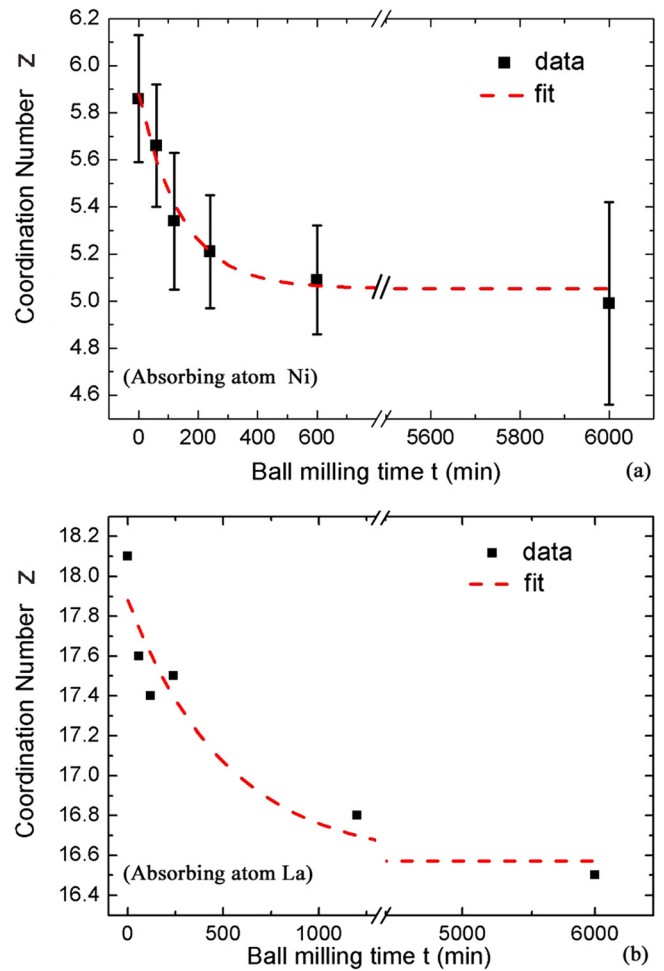


FIG. 3. Number of nearest neighbours Z of Ni (a) and of La (b) as a function of ball milling time measured by means of EXAFS. The dashed lines represent exponential fits to the data according to Eq. (1).

the data yields $\beta_{\Delta H} = (5.5 \pm 2.2) \cdot 10^{-7}$ per impact, $\Delta H_{BM}^{max} = 4.8 \pm 0.7 \text{ J/g}$, and $\Delta H_{aa}^{max} = 9.8 \pm 0.6 \text{ J/g}$. The maximum releases ΔH_{BM}^{max} and ΔH_{aa} are of about the same magnitude.

TABLE I. Number of Al nearest neighbours around Ni and La, $Z(\text{Ni})$ and $Z(\text{La})$, respectively, interatomic distance, D , and mean squared relative displacement of the effective interatomic distance, σ^2 , of $\text{Al}_{85}\text{Ni}_{10}\text{La}_5$ powder in the as-atomized state and after ball milling to different times, obtained by fitting the data with a single-shell model.

Ball milling time	Absorbing atom	$Z(\text{Ni})$	$D(\text{\AA})$	$\sigma^2(\text{\AA}^2)$
(As atomized)	Ni	5.9(3)	2.44(1)	0.010(1)
60 min	Ni	5.7(3)	2.44(1)	0.009(1)
120 min	Ni	5.3(3)	2.44(1)	0.009(1)
240 min	Ni	5.2(2)	2.44(1)	0.009(1)
600 min	Ni	5.1(2)	2.44(1)	0.009(1)
6000 min	Ni	5.0(4)	2.43(1)	0.009(2)
120 min + 15 min@150°C	Ni	5.5(4)	2.44(1)	0.009(1)
(As atomized)	La	18.1 ± 2.6	3.37(5)	0.018(3)
60 min	La	17.6 ± 1.3	3.35(3)	0.018(1)
120 min	La	17.4 ± 1.4	3.36(3)	0.018(2)
240 min	La	17.5 ± 1.6	3.36(3)	0.018(2)
1200 min	La	16.8 ± 1.5	3.34(3)	0.018(2)
6000 min	La	16.5 ± 1.4	3.35(3)	0.018(2)

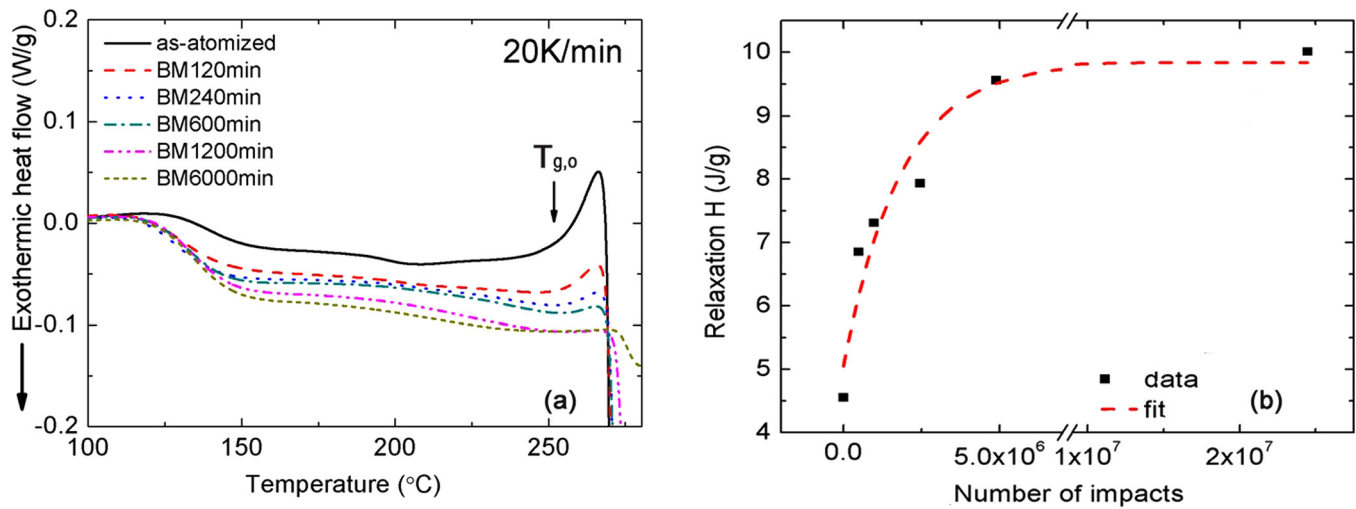


FIG. 4. (a) DSC trace of Al₈₅Ni₁₀La₅ powder in the as-atomized condition and after ball milling to different times from 100 °C to 280 °C at a heating rate of 20 K/min (a), total heat release obtained by integration of the DSC curve from 100 °C to $T_{g,0}$ as a function of the number of impacts n according to Eq. (2).

IV. DISCUSSION

Van den Beukel *et al.*²⁴ and Koebrugge *et al.*²⁵ pointed out that the variation in relaxation enthalpy is proportional to the variation in excess free volume. The free volume induced by plastic deformation is located within such shear bands.²⁶ The excess heat which is released below $T_{g,0}$ in the ball-milled Al₈₅Ni₁₀La₅ powder is therefore due to the excess free volume induced by plastic deformation that in metallic glasses proceeds via shear bands. As ΔH_{BM}^{max} and ΔH_{aa} are of about the same magnitude, the maximum free volume induced by plastic deformation at room temperature has about the same magnitude as the free volume in the as-atomized condition.

Creation and annihilation of free volume inside shear bands of Zr-based alloys were quantified by Ritter and Albe²⁶ using molecular dynamics simulation. They found that the highly strained material inside the shear bands contains appreciable amounts of excess free volume, while the surrounding material experiences a compressive strain due to the dilatation of the shear band. Thermal treatment results in the annihilation of free volume inside the shear bands with the surrounding material in the matrix being under compression.

The low coordination number $Z_{Ni} \approx 6$ in the as-atomized condition is ascribed to the strongly covalent character of the Ni-Al bonds reflected by the small Ni-Al distance ($D = 244$ pm, see Table I) which is 10% shorter than the sum of the metallic radii of Ni ($r(Ni) = 125$ pm (Ref. 27)) and Al ($r(Al) = 143$ pm (Ref. 27)). Strong bond shortening has been reported for several Al-TM-RE amorphous alloys (TM: transition metal, RE: rare-earth metal) and was ascribed to the strongly covalent character of TM-Al bonds caused by charge transfer from Al atoms to TM atoms, which induces a decrease in atomic size of the TM atoms and an increase in atomic size of the Al atoms in the alloy.^{28–33} Such changes in atomic diameters give rise to the coordination number of $Z_{Ni} \approx 6$ around Ni.^{28–33} Matsubara *et al.*³⁴ reported a value of 6.5 ± 0.2 Al nearest neighbors and 2.2 ± 1.7 Y nearest neighbors around Ni, measured in

Al₈₇Ni₈Y₅ metallic glass by anomalous X-ray scattering. The large uncertainty in the number of Y nearest neighbors around Ni allows for a local order around Ni which is approximately the same as in Al₈₅Ni₁₀La₅.

The value of $Z_{Ni} \approx 6$ is low compared to the value of $Z = 10.9$ for dense random packing of hard spheres (DRPHS)³⁵ in which the atomic diameters for Ni and Al from Ref. 27 are used. Miracle^{36,37} established an efficient packing model for which solute-centred clusters serve as structural units in metallic glasses. This model describes the coordination number of a solute as a function of the ratio of the radius of solute atoms to the radius of solvent atoms, using atomic radii deduced from pure crystals. The use of these radii naturally results in coordination numbers which are close to those for the competing crystalline structures. The results of this model are, therefore, in direct conflict to the results of the present and other studies^{28–33} which report only about 6 Al nearest neighbors around transition metal atoms.

Saksl *et al.* used two-shell model in order to fit their EXAFS data on rare earth edge.³³ In this work, the FT spectra on La edge show narrow peaks which are unlikely contributed by two paths with different bond lengths. Indeed, the values of σ^2 for the single shell fit are sufficiently small (see Table I) to describe the local structure around La by one shell only.

Contrary to Ni-Al, the La-Al bond distance in Al₈₅Ni₁₀La₅ metallic glass is of the same size ($D = 331$ pm) as the sum of the atomic radii ($r(La) = 188$ pm, $r(Al) = 143$ pm (Ref. 27)), giving rise to a coordination number ($Z(La) \approx 18$) in the as-atomized state which within the experimental accuracy is in agreement with the predictions from the DRPHS model³⁵ ($Z_{DRPHS}(La) = 17.1$).

The decrease in coordination number from ≈ 6 to ≈ 5 for Ni and from 18.1 to 16.5 for La during milling points at the formation of free volume in the first shell of the solute-centred clusters as schematically depicted in Fig. 5 for Ni. Following the analysis of Ritter and Albe,²⁶ the formation of free volume and hence the decrease in coordination number during plastic deformation occurs in shear bands and the

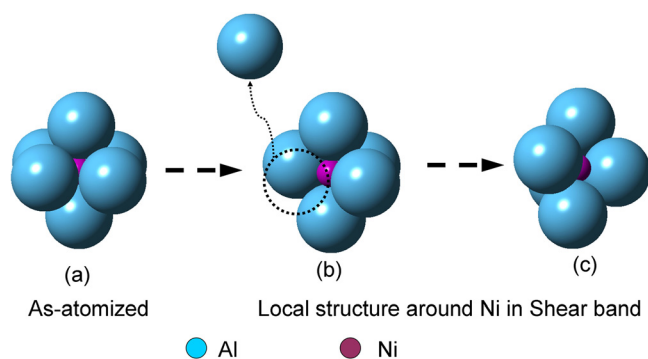


FIG. 5. Local structure around Ni with neighboring Al atoms in the as-atomized condition (a), free volume induced during ball milling (b), and free volume shrunk since randomly packed by 5 Al atoms (c).

coordination numbers of Ni and La in $\text{Al}_{85}\text{Ni}_{10}\text{La}_5$ will recover at least partly during continuous heating up to $T_{g,o}$ and approach their initial values in the as-atomized state. After annealing for 15 min, the maximum of the EXAFS spectrum increased, see inset of Fig. 1, indicating a recovery process in the shear bands.

Though our measurements provide clear evidence of changes in coordination numbers around absorbing atoms during ball milling, the details of the distribution of the free volume around an absorbing atom cannot be deduced from our measurements. As the total free volume in a metallic glass is generally of the order of a few per cent of the sample volume, the mean free volume assigned to a particular atom is much less than one atomic volume while vacancy-like defects do rarely exist. The amount of vacancy-like defects can, however, strongly increase during plastic deformation. According to the free volume model of Spaepen,¹² vacancy-like defects are created at high stress levels during creep deformation by squeezing atoms into neighboring holes with size less than an atomic volume leaving behind holes of one atomic size, i.e., vacancy-like defects. At sufficiently high temperature, the creation of vacancy-like defects competes with a relaxation process that tends to annihilate the extra free volume created and to restore the system to its initial structure.¹² At sufficiently low temperatures and high deformation rates, plastic deformation of metallic glasses proceeds in shear bands. Two scenarios may be considered to describe the evolution of defects within the shear bands depending on the local heat created.

(i) The heat created within the shear bands is low compared to T_g . In this case, rearrangement of the defect structure will not occur and the deformation-induced vacancy-like defects are stable. This process may be compared to low temperature irradiation of a metallic glass with fast electrons where the energy transferred from an electron to an atom in the glass is sufficiently high to displace the atom from its initial site leaving behind a vacancy-like defect. The creation of vacancy-like defects by irradiation with fast electrons has been observed by positron annihilation lifetime spectroscopy measurements in different amorphous alloys.^{38–40} Such defects annihilate gradually during thermal treatment, which results in a predominantly diffusive distribution of the free volume.

(ii) The heat created within the shear bands is sufficiently high to exceed the glass temperature above which the material behaves like a liquid. In liquids, thermal expansion due to temperature increase is caused by an increase in the equilibrium concentration of vacancies accompanied by a decrease in coordination number rather than by an increase in nearest neighbour distance.^{41–44} For example, the coordination number of Ni in liquid Ni increases from 11.2 to 12.3 when the temperature decreases from 1905 K to 1435 K while changes in interatomic distance in liquid Ni are small compared to those in crystalline Ni at similar temperature increments.⁴⁴ Moreover, in molten Si where the bonds have a more covalent character than in pure metals an increase in Z from 4.9 at 1893 K to 6.1 at 1403 K was observed while changes in interatomic distance were again small.⁴⁵ We therefore conclude that the decrease in Z from ≈ 6 to ≈ 5 in $\text{Al}_{85}\text{Ni}_{10}\text{La}_5$ during ball-milling results either from an increase in the shear band temperature by several hundred K, thus notably exceeding the glass transition temperature, or by plastic deformation at sufficiently low temperatures that do not allow for structural relaxation. Above T_g , the alloy behaves like a liquid and within a short time the material approaches its structural equilibrium followed by a quench to the matrix temperature during which the structure is frozen-in.¹⁸ This interpretation is supported by the results of Zhao and Li⁴⁶ who determined the temperature increase in alloy $\text{Zr}_{41.25}\text{Ti}_{13.75}\text{Ni}_{10}\text{Cu}_{12.5}\text{Ni}_{22.5}$ (commercial name Vitreloy 1) by finite element calculations and found that the strain rate notably affects local heating. They also found that compression causes a higher temperature increase than tension.

Strain rate dependent internal heating in shear bands was confirmed by Liu and Liu⁴⁷ who calculated thermal heating analytically. When the strain rate exceeds $6 \times 10^3 \text{ s}^{-1}$, the temperature within shear bands rises to above T_g within a short time period followed by a quench to ambient temperature. The deformation rate during ball milling in a SPEX mixer mill was estimated to $\approx 10^4 \text{ s}^{-1}$, which supports our conclusion that the temperature in the shear bands of $\text{Al}_{85}\text{Ni}_{10}\text{La}_5$ alloy exceeds the glass transition temperature for a short time and the alloy approaches a structural state characterized by a lower number of nearest neighbours before it is quenched to room temperature by the surrounding matrix.

Applying such a thermal spike model to ball milling of $\text{Al}_{85}\text{Ni}_{10}\text{La}_5$ powder, the creation of vacancies in the first shell around Ni and La at $T > T_g$ within the shear band leads to a decrease in the number of Al ligands around Ni and La. The high mobility of atoms in the shear bands⁴⁸ during their genesis may lead to redistribution of the contact atoms of Ni and La, which leads to a more diffusive structure of the free volume. The displacement of Al atoms may lead to their agglomeration between the clusters, which finally results in nucleation and growth of Al-crystals with size of the order of 10 nm as reported previously.^{18,23} Investigation of the structure of heavily deformed and amorphized Ni-Nb-Y alloy with “solite-solvent” short range order shows grainy structure with grain size $\sim 20 \text{ nm}$.⁴⁹

Changes in coordination number have also been reported by Cao *et al.*⁵⁰ who observed by MD simulation a reduction of Z around Cu from 12 to 9 within the shear bands of plastically deformed Cu-Zr metallic glass. The change in the coordination number of Ni and La in $\text{Al}_{85}\text{Ni}_{10}\text{La}_5$ during plastic deformation requires a bond breaking mechanism operating in the shear bands during deformation. Such a mechanism has been suggested by both Suzuki *et al.*⁵¹ and by Revesz *et al.*⁵² to explain structural anisotropy after anelastic creep and after high pressure torsion, respectively.

As Ni- and La-centred atomic clusters in the as-atomized condition are tightly and densely packed,⁵³ the free volume in as-atomized powder is mainly located in between these clusters.^{2,4} It is in such solvent-rich configurations between dense, tightly bound solute-centred clusters where elastic strain is preferentially located, while the solute-centred clusters are less affected by elastic deformation.^{1,2,4} This might lead to the conclusion that plastic deformation mainly alters the structure of the solvent-rich configurations between tightly bound solute-centred clusters, while the solute-centred clusters themselves are less affected.⁴ In $\text{Al}_{85}\text{Ni}_{10}\text{La}_5$ metallic glass, however, plastic deformation causes appreciable structural changes in the tight Ni- and La-centred clusters, thus suggesting a different displacement mechanism being effective in $\text{Al}_{85}\text{Ni}_{10}\text{La}_5$ metallic glass.

In order to describe the decrease of Z for Ni and La quantitatively, we apply a shear band model in which $Z = Z_{sb}$ inside a shear band and $Z = Z_{aa}$ in the undamaged as-atomized condition outside the shear bands. Maximum damage is assumed in each of the shear bands, i.e., an overlap of shear bands formed in a given state of deformation with previously existing ones will not cause further damage in the overlapping regions, see Fig. 6. This assumption changes the linear decrease with n of the volume $V_{aa}(n)$ of the as-atomized powder outside the shear bands as expected for non-overlapping shear bands to an exponential decay⁵⁴

$$V_{aa}(n) = V_{aa}^0 \exp(-\beta n), \quad (3)$$

where $V_{aa}^0 = V_{aa}(n=0)$ denotes the volume of the as-atomized powder and a parameter β describes the relative amount of shear band volume created per impact and contains the number k of shear bands per impact and the volume v of a single shear band

$$\beta = kv. \quad (4)$$

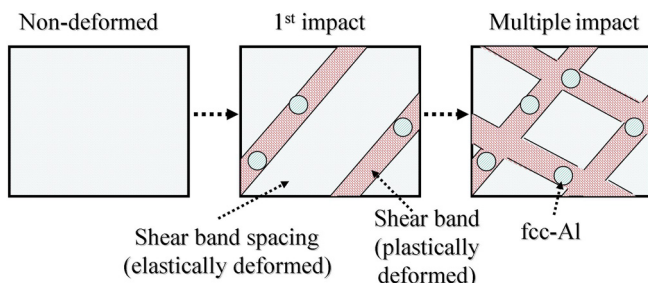


FIG. 6. Schematic view of the changes in microstructure by creation of shear bands during ball milling.

Taking account of the relation $V_{aa}(n) + V_{sb}(n) = V_{aa}^0$, the total volume $V_{sb}(n)$ of shear bands after using Eq. (3) can be written as

$$V_{sb}(n) = V_{aa}^0 \cdot [1 - \exp(-\beta \cdot n)]. \quad (5)$$

The average coordination number Z of Ni or La in the specimen is given by

$$Z(n) = \{V_{aa}(n) \cdot Z_{aa} + V_{sb}(n) \cdot Z_{sb}\} / V_{aa}^0, \quad (6)$$

where Z_{aa} and Z_{sb} denote the coordination numbers of solute-centred cluster in the as-atomized condition and in the shear band, respectively. Using Eqs. (3) and (5), Eq. (6) can be written as

$$Z(n) = Z^{sb} + \Delta Z \cdot \exp(-\beta \cdot n), \quad (7)$$

where $Z = Z_{aa} - Z_{sb}$. Hence, the changes of both the shear band volume and the coordination numbers of Ni and La should follow exponential functions with the same parameter β . Fitting the data in Fig. 3 by Eq. (7) yields $\beta_{Ni} = 1.7(4) \times 10^{-6}$, $Z_{sb} = 5.1(1)$ and $\Delta Z_{Ni} = 0.8(1)$. Hence, $Z_{Ni} = 5.9$ in the as-atomized condition ($n=0$) and approaches a value of 5.1 for infinitely long milling times. A fit to the data of Z_{La} , see Fig. 3(b), yields $\beta_{La} = 2.9(7) \times 10^{-7}$, $Z_{La}^{sb} = 16.6(1)$ and $\Delta Z_{La} = 1.3(1)$. Due to the large experimental uncertainties especially for β_{La} , a direct comparison of β_{Ni} and β_{La} is difficult. Therefore, we use $\beta_{\Delta H}$ which lies in between. The experimental data are compatible with the viewpoint that all these beta values are the same. For the description of the evolution of shear bands during ball milling, we used the value of $\beta_{\Delta H}$ obtained from Eq. (1). This value should also describe the recovery of both Z_{Ni} and Z_{La} during thermal treatment to the glass transition.

The quantitative description of the changes in Z within a shear band model allows us to compare our model with the Hertz model.⁵⁵ The volume of shear bands created by the first ball-vial impact can be approximated by linearising Eq. (3) to $V_{aa}(n) = V_{aa}^0 (1 - \beta)$ and using $\beta_{\Delta H} = (5.5 \pm 2.2) \times 10^{-7}$ deduced from the heat release measurements. This yields $V_{sb}(n=1) = 9.7 \times 10^{-7} \text{ cm}^3$. The volume of plastic deformation calculated applying the Hertz model⁵⁵ yields $V_{Hertz} = 6.7 \times 10^{-4} \text{ cm}^3$ using the parameters given in Table II. A comparison of V_{Hertz} and $V_{sb}(n=1)$ suggests that a fraction $\gamma = 1.4 \times 10^{-3}$ of V_{Hertz} is occupied by shear bands. This is in line with the fact that only a small volume fraction is attained by shear bands while other parts of the particle are deformed just elastically. Assuming a typical shear band

TABLE II. The parameters used in Hertz model for SPEX mixer mill with ZrO_2 balls and ZrO_2 container where r_B is the radius of each ball, s is the velocity of collision, ρ_B is the density of the balls, E is the Young's modulus of the collision body, L is the length of the mill, ρ_P is the density of the powder, C_R is the mass ratio of balls and powder, D_m is the diameter of the mill container, and m_B is the number of balls.

r_B	s	ρ_B	E	L	ρ_P	C_R	D_m	m_B
0.64 cm	3.9 m/s	5.68 g/cm ³	200 GPa	4 cm	3.5 g/cm ³	2	4 cm	2

thickness of 10 nm for our particle size,⁸ a value of 7.1 μm for the shear band spacing is deduced. This value differs by a factor of 5.5 from the value reported by Conner *et al.*⁵⁶ for 11 μm -thick ribbons and wires, which roughly corresponds to the mean particle size of our $\text{Al}_{85}\text{Ni}_{10}\text{La}_5$ powder. The discrepancy could have been caused by the spherical morphology of the $\text{Al}_{85}\text{Ni}_{10}\text{La}_5$ powder particles used in our experiment. Furthermore, we used one shear band thickness and one shear band spacing for the above estimation. Many metallic glasses, however, exhibit sub-band structures with notably smaller shear band thicknesses.^{57–59} The presence of sub-shear band structures in plastically deformed $\text{Al}_{85}\text{Ni}_{10}\text{La}_5$ powder particles would therefore decrease the discrepancy between the present results and Hertz model.

V. CONCLUSIONS

The number of nearest neighbours around nickel and lanthanum atoms in glassy $\text{Al}_{85}\text{Ni}_{10}\text{La}_5$ powder decreases with progressing plastic deformation carried out by ball milling while the interatomic distance and the mean square displacement of nearest neighbours around Ni and La atoms do not change. These changes point at the creation of free volume around Ni and La atoms. The structural changes are described by a shear band model in which maximum damage is achieved in each shear band while outside the shear bands the initial structural state of the as-atomized powder is sustained. The numbers of nearest neighbours recover at least partly upon thermal treatment. These changes in structure by plastic deformation strongly resemble those of a liquid when its temperature is increased, pointing at adiabatic heating in the shear bands to temperatures above T_g . The high mobility of atoms within the shear band during adiabatic heating enables the newly created Al interstitials to agglomerate with other Al atoms in the solvent-rich regions, thus forming Al fcc nanocrystals by nucleation and growth.

Contrary to elastic deformation which is believed to occur in solvent-rich areas of the alloy accompanied by only minor structural changes of the solute-centred clusters,¹ plastic deformation at high strain rate strongly affects SRO in solute-centred clusters by reducing the number of nearest neighbours of the solute atoms.

Taking typical values for the width and spacing of shear bands from the literature, our results agree within a factor of 5.5 with the Hertz impact theory for contact mechanics that describes the deformation of a powder in a mill.

ACKNOWLEDGMENTS

The authors would like to thank C. Förster, C. Leistner, and H. Stapel for their help in specimen preparation and for support during the ball milling experiments. We would also like to thank Dr. Klaumünzer (HZB) for stimulating discussions. Support of one of the authors (Yao Liu) by the Postdoctoral Science Foundation of China (Grant No. 2014M551900), the Shandong Provincial Natural Science Foundation, China (Grant No. ZR2013EMQ010) and Independent Innovation Foundation of Shandong University (Grant No. 2013HW001) is gratefully acknowledged.

- ¹J. C. Ye, J. Lu, C. T. Liu, Q. Wang, and Y. Yang, *Nature Mater.* **9**, 619 (2010).
- ²D. Ma, A. D. Stoica, X. L. Wang, Z. P. Lu, B. Clausen, and D. W. Brown, *Phys. Rev. Lett.* **108**, 085501 (2012).
- ³W. Dmowski, T. Iwashita, C. P. Chuang, J. Almer, and T. Egami, *Phys. Rev. Lett.* **105**, 205502 (2010).
- ⁴W. H. Wang, *Nature Mater.* **11**, 275 (2012).
- ⁵C. A. Schuh, T. C. Hufnagel, and U. Ramamurty, *Acta Mater.* **55**, 4067 (2007).
- ⁶M. Q. Jiang, W. H. Wang, and L. H. Dai, *Scr. Mater.* **60**, 1004 (2009).
- ⁷Q. K. Li and M. Li, *Appl. Phys. Lett.* **88**, 241903 (2006).
- ⁸Y. Zhang and A. L. Greer, *Appl. Phys. Lett.* **89**, 071907 (2006).
- ⁹P. E. Donovan and W. M. Stobbs, *Acta Metall.* **29**, 1419 (1981).
- ¹⁰R. W. Cahn, N. A. Pratten, M. G. Scott, H. R. Sinning, and L. Leonardsson, *Symposium F—Rapidly Solidified Metastable Materials* (MRS Proceedings, 1984), Vol. 28, p. 241.
- ¹¹G. Wilde and H. Rosner, *Appl. Phys. Lett.* **98**, 251904 (2011).
- ¹²F. Spaepen, *Acta Metall.* **25**, 407 (1977).
- ¹³A. S. Argon and H. Y. Kuo, *Mater. Sci. Eng.* **39**, 101 (1979).
- ¹⁴H. Chen, Y. He, G. J. Shiflet, and S. J. Poon, *Nature* **367**, 541 (1994).
- ¹⁵W. H. Jiang, F. E. Pinkerton, and M. Atzmon, *J. Appl. Phys.* **93**, 9287 (2003).
- ¹⁶W. H. Jiang and M. Atzmon, *Acta Mater.* **51**, 4095 (2003).
- ¹⁷J. J. Lewandowski and A. L. Greer, *Nature Mater.* **5**, 15 (2006).
- ¹⁸J. Vierke, G. Schumacher, M. Balog, J. Nagy, F. Simancik, M. Wollgarten, and J. Banhart, *Mater. Sci. Eng., A* **558**, 64 (2012).
- ¹⁹L. Gerking, *Powder Metall. Int.* **25**, 59 (1993).
- ²⁰M. Newville, *J. Synchrotron. Radiat.* **8**, 96 (2001).
- ²¹B. Ravel, *J. Synchrotron. Radiat.* **8**, 314 (2001).
- ²²J. J. Rehr, J. M. Deleon, S. I. Zabinsky, and R. C. Albers, *J. Am. Chem. Soc.* **113**, 5135 (1991).
- ²³Y. Liu, G. Schumacher, S. Zimmermann, and J. Banhart, *J. Alloys Compd.* **509**, S78 (2011).
- ²⁴A. van den Beukel and J. Sietsma, *Acta Metall. Mater.* **38**, 383 (1990).
- ²⁵G. W. Koebrugge, J. Sietsma, and A. van den Beukel, *Acta Metall. Mater.* **40**, 753 (1992).
- ²⁶Y. Ritter and K. Albe, *Acta Mater.* **59**, 7082 (2011).
- ²⁷N. F. Henry and K. Lonsdale, *International Tables for X-ray Crystallography*, 3rd ed. (Kynock Press, Birmingham, England, 1969).
- ²⁸A. N. Mansour, A. Marcelli, G. Cibin, G. Yalovega, T. Sevastyanova, and A. V. Soldatov, *Phys. Rev. B* **65**, 134207 (2002).
- ²⁹A. N. Mansour, C. P. Wong, and R. A. Brizzolaro, *Phys. Rev. B* **50**, 12401 (1994).
- ³⁰K. Saksl, P. Jovari, H. Franz, and J. Z. Jiang, *J. Appl. Phys.* **97**, 113507 (2005).
- ³¹W. Zalewski, J. Antonowicz, R. Bacewicz, and J. Latuch, *J. Alloys Compd.* **468**, 40 (2009).
- ³²H. Y. Hsieh, B. H. Toby, T. Egami, Y. He, S. J. Poon, and G. J. Shiflet, *J. Mater. Res.* **5**, 2807 (1990).
- ³³K. Saksl, P. Jóvári, H. Franz, Q. S. Zeng, J. F. Liu, and J. Z. Jiang, *J. Phys. Condens. Matter.* **18**, 7579 (2006).
- ³⁴E. Matsubara, Y. Waseda, A. Inoue, H. Ohtera, and T. Masumoto, *Z. Naturforsch.* **44**, 814 (1989).
- ³⁵V. Vitek, *Amorphous Materials: Modeling of Structure and Properties: Proceedings of Symposium* (Metallurgical Society of AIME, Warrendale, PA, 1983), pp. viii, 347 p.
- ³⁶D. B. Miracle, *Nature Mater.* **3**, 697 (2004).
- ³⁷D. B. Miracle, *Acta Mater.* **54**, 4317 (2006).
- ³⁸P. Moser, P. Hautajärvi, J. Yli-Kauppila, and C. Corbel, *Radiat. Eff. Def. Solids* **62**, 153 (1982).
- ³⁹J. Yli-Kauppila, P. Moser, and H. Kiinzi, *Appl. Phys. A* **27**, 31 (1982).
- ⁴⁰Y. Petrusenko, A. Bakai, V. Borysenko, A. Astakhov, and D. Barankov, *Intermetallics* **17**, 246 (2009).
- ⁴¹S. Takeuchi, *Mater. Trans. JIM* **30**, 647 (1989).
- ⁴²G. Jacobs and I. Egry, *Phys. Rev. B* **59**, 3961 (1999).
- ⁴³N. A. Mauro, J. C. Bendert, A. J. Vogt, J. M. Gewin, and K. F. Kelton, *J. Chem. Phys.* **135**, 044502 (2011).
- ⁴⁴I. Egry and D. Holland-Moritz, *Eur. Phys. J. Spec. Top.* **196**, 131 (2011).
- ⁴⁵H. Kimura, M. Watanabe, K. Izumi, T. Hibiya, D. Holland-Moritz, T. Schenk, K. R. Bauchspieß, S. Schneider, I. Egry, K. Funakoshi, and M. Hanfland, *Appl. Phys. Lett.* **78**, 604 (2001).
- ⁴⁶M. Zhao and M. Li, *Scr. Mater.* **65**, 493 (2011).
- ⁴⁷W. D. Liu and K. X. Liu, *Appl. Phys. Lett.* **100**, 141904 (2012).
- ⁴⁸J. Bokeloh, S. V. Divinski, G. Replitz, and G. Wilde, *Phys. Rev. Lett.* **107**, 269901 (2011).
- ⁴⁹A. A. Mazilkin, G. E. Abrosimova, S. G. Protasova, B. B. Straumal, G. Schütz, S. V. Dobatkin, and A. S. Bakai, *J. Mater. Sci.* **46**, 4336 (2011).

- ⁵⁰A. J. Cao, Y. Q. Cheng, and E. Ma, *Acta Mater.* **57**, 5146 (2009).
- ⁵¹Y. Suzuki, J. Haimovich, and T. Egami, *Phys. Rev. B* **35**, 2162 (1987).
- ⁵²A. Revesz, E. Schafler, and Z. Kovacs, *Appl. Phys. Lett.* **92**, 011910 (2008).
- ⁵³T. Egami, S. J. Poon, Z. Zhang, and V. Keppens, *Phys. Rev. B* **76**, 024203 (2007).
- ⁵⁴J. W. Christian, *The Theory of Transformations in Metals and Alloys*, 3rd ed. (Pergamon, Oxford, 2002).
- ⁵⁵D. R. Maurice and T. H. Courtney, *Metall. Mater. Trans. A* **21**, 289 (1990).
- ⁵⁶R. D. Conner, W. L. Johnson, N. E. Paton, and W. D. Nix, *J. Appl. Phys.* **94**, 904 (2003).
- ⁵⁷Y. H. Liu, G. Wang, R. J. Wang, D. Q. Zhao, M. X. Pan, and W. H. Wang, *Science* **315**, 1385 (2007).
- ⁵⁸J. Schroers and W. L. Johnson, *Phys. Rev. Lett.* **93**, 255506 (2004).
- ⁵⁹B. A. Sun and W. H. Wang, *Appl. Phys. Lett.* **98**, 201902 (2011).